A mechanism of internal decadal atlantic ocean variability in a high-resolution coupled climate model

Article

Accepted Version

Menary, M. B., Hodson, D. L. R. ORCID: https://orcid.org/0000-0001-7159-6700, Robson, J. I. ORCID: https://orcid.org/0000-0002-3467-018X, Sutton, R. T. ORCID: https://orcid.org/0000-0001-8345-8583 and Wood, R. A. (2015) A mechanism of internal decadal atlantic ocean variability in a high-resolution coupled climate model. Journal of Climate, 28 (19). pp. 7764-7785. ISSN 1520-0442 doi: https://doi.org/10.1175/JCLI-D-15-0106.1 Available at https://centaur.reading.ac.uk/40809/

www.reading.ac.uk/centaur

CentAUR

Central Archive at the University of Reading

Reading's research outputs online

A mechanism of internal decadal variability in a high resolution coupled climate model

Matthew B. Menary[*]

Met Office Hadley Centre, United Kingdom

Daniel L. R. Hodson, Jon I. Robson and Rowan T. Sutton

NCAS-Climate, University of Reading, United Kingdom

Richard A. Wood

Met Office Hadley Centre, United Kingdom

[*]*Corresponding author address:* Matthew B. Menary, Met Office Hadley Centre, Met Office, Fitzroy Road, Exeter, Devon, EX1 3PB. United Kingdom.

E-mail: matthew.menary@metoffice.gov.uk

ABSTRACT

The North Atlantic Ocean subpolar gyre (NA SPG) is an important region for initialising decadal climate forecasts. Climate model simulations and palaeo climate reconstructions have indicated that this region could also exhibit large, internally generated variability on decadal timescales. Understanding these modes of variability, their consistency across models, and the conditions in which they exist, is clearly important for improving the skill of decadal predictions — particularly when these predictions are made with the same underlying climate models. Here we describe and analyse a mode of internal variability in the NA SPG in a state-of-the-art, high resolution, coupled climate model. This mode has a period of 17 years and explains 15–30% of the annual variance in related ocean indices. It arises due to the advection of heat content anomalies around the NA SPG. Anomalous circulation drives the variability in the southern half of the NA SPG, whilst mean circulation and anomalous temperatures are important in the northern half. A negative feedback between Labrador Sea temperatures/densities and those in the North Atlantic Current is identified, which allows for the phase reversal. The atmosphere is found to act as a positive feedback on to this mode via the North Atlantic Oscillation which itself exhibits a spectral peak at 17 years. Decadal ocean density changes associated with this mode are driven by variations in temperature, rather than salinity — a point which models often disagree on and which we suggest may affect the veracity of the underlying assumptions of anomaly-assimilating decadal prediction methodologies.

2

1. Introduction

The North Atlantic Ocean has been shown to be a key region for the initialisation of decadal forecasts (Dunstone et al. 2011) and sea surface temperatures (SSTs) in this region are likely important for the climates of the nearby continents of North America and Europe (Rodwell et al. 1999). SSTs in the North Atlantic show large multidecadal variability (Knight et al. 2005) which has been linked to drought in the Sahel region (Folland et al. 1986; Zhang and Delworth 2006), Atlantic hurricane formation (Goldenberg et al. 2001; Smith et al. 2010), precipitation over northern Europe (Sutton and Hodson 2005), and the growth and persistence of Arctic sea ice, which could also affect the climate of northern Europe (Screen 2013). In addition to the response to globally increasing greenhouse gas emissions, understanding the natural variability of this region is important in helping to improve the veracity of decadal predictions, which rely in particular on the North Atlantic subpolar gyre (NA SPG) (Dunstone et al. 2011). Indeed, the NA SPG could be an important region in regulating decadal (Hakkinen and Rhines 2004) and longer timescale climate cycles (Kleppin et al. 2015). Due to the paucity of long observational records within the NA SPG much of the mechanistic understanding must be gained through analysis of climate models, some of which is now summarised.

There have been many studies investigating the interannual/decadal variability of the NA SPG, which may be useful in adding value to predictions made up to a decade ahead. Given the number of such studies we present here a very brief review. One of the first studies into NA SPG decadal variability proposed a mechanism related to temperature induced gyre changes which advect salinity into the model's sinking regions and had a periodicity of 50 years in an early coupled climate model (Delworth et al. 1993). Following on from the idealised-ocean work of Frankignoul et al. (1997) this mechanism was ocean-only with the atmosphere providing white noise forcing.

3

However, the agreement between idealised models and fully coupled general circulation models was better in the subtropics than subpolar regions (Frankignoul et al. 1997). Later work found the mechanism of Delworth et al. (1993) in the HadCM3 model (Dong and Sutton 2005) but with a reduced period of just 25 years with this reduction attributed in part to the removal of flux corrections and the improved representation of surface temperature gradients in the ocean.

Using the ECHAM3/LSG model Timmermann et al. (1998) searched for the observationally-based salinity-dominated mechanism of Wohlleben and Weaver (1995) related to great salinity anomalies. A periodicity of 35 years was reported and this time the atmosphere was postulated to play a direct, coupled role. However, in parallel work using a coupled model with the same atmosphere but a different ocean (ECHAM3/HOPE), Grotzner et al. (1998) also suggested a coupled decadal mode, but with the now even shorter timescale of 17 years, and this time with temperature changes playing an important role. To try and reconcile these differences, Eden and Willebrand (2001) investigated the relative importance of heat and freshwater fluxes related to the North Atlantic Oscillation (NAO) in an ocean-only model and found that, of the two, heat fluxes were more important than freshwater fluxes for the interannual/decadal variability of the NA SPG. However, the coupling between the ocean and atmosphere on multiannual timescales appears to go in both directions (Rodwell et al. 1999; Battisti et al. 1995) suggesting that coupled models are required in order to fully capture the interactions.

Disagreements remain over the main contribution to density changes in the NA SPG, along with questions about the degree to which the atmosphere plays a coupled role and the key processes which set the timescale. However, the general periodicity of simulated multiannual but sub-centennial variability has begun to crystallise (Frankcombe et al. 2010). In addition to the aforementioned works, other studies of this variability within the NA SPG continually find periodicities near to 20 years (Visbeck et al. 1998; Watanabe et al. 1999; Holland et al. 2001; Eden

4

and Greatbatch 2003; Dai et al. 2005; Alvarez-Garcia et al. 2008; Danabasoglu 2008; Born and Mignot 2012; Tulloch and Marshall 2012; Sévellec and Fedorov 2013; Escudier et al. 2013; Kwon and Frankignoul 2014). This timescale is sometimes attributed to the basin-crossing timescale of Rossby waves in the NA SPG (Frankcombe et al. 2010) though many studies attribute it to the time to build up sufficient temperature anomalies. Indeed, the role of the forcing from Rossby waves has recently been called into question (MacMartin et al. 2013) and the importance of wave processes in controlling decadal variability is still unclear (Fevrier et al. 2007; Roussenov et al. 2008). This approximately 20 year variability is generally separate from centennial variability in the Atlantic, which relies on the long advective timescales to bring anomalies from the tropical Atlantic or Arctic and in which salinity is more consistently the dominant driver of the related density changes (Vellinga and Wu 2004; Jungclaus et al. 2005; Menary et al. 2012). Indeed, the role of salinity in either weakening or strengthening circulations in the NA SPG may depend on timescale (Deshayes et al. 2014).

As previously noted, limited instrumental observations within the NA SPG make it hard to detect the existence of decadal variability. However, palaeo reconstructions do suggest increased variance at decadal timescales (Mann et al. 1995) and indeed 20 year variability can be detected on the outskirts of the NA SPG in palaeo proxies (Chylek et al. 2012). Additionally, the relative importance of temperature or salinity variability in real world overturning circulation changes has been investigated. On multiannual timescales, Curry and McCartney (2001) found that the Labrador Sea potential energy anomaly and the overturning were thermally driven — insofar as temperatures changed twice as much as salinities in the sinking regions (after scaling by the thermal and haline expansion coefficients).

To bring together this previous work with climate models, Figure 1 schematically depicts the studies so far mentioned along with the reported period and whether the proposed mechanism

5

is coupled or ocean-only. Additionally, whether the timescale is reported to be primarily set by either wave processes; the mean circulation strength and the integration of anomalies within the NA SPG; or interaction with the deep western boundary current is noted. Also noted is whether density changes in the Labrador Sea (or model equivalent sinking region) are reported to be temperature or salinity dominated. In short, there is much disagreement between the models on the key processes, the details of the mechanism (see above for some examples; the reader is referred to the specific studies for further details), the degree of atmospheric interaction, and the dominant driver of density changes.

As analysing decadal variability requires many decades/centuries of integration these previous studies generally use low resolution coupled models ($>1°$ ocean resolution, $>2°$ atmosphere resolution) or higher resolution ocean-only models. There are reasons to suppose that improved atmospheric resolution could affect the amplitude of decadal variability (Danabasoglu 2008) whilst improved ocean resolution and associated representation of the Gulf Stream and other boundary currents may affect the precise timescales of multiannual/decadal variability (Grotzner et al. 1998; Gelderloos et al. 2011; Hodson and Sutton 2012). Higher resolution topography may also be expected to affect the efficacy of wave processes as compared to idealised ocean models with smoothed/no topography (Roussenov et al. 2008; Zhang and Vallis 2007) and improve deep water pathways (Spence et al. 2011). At high ocean resolution eddy induced mixing can be left explicit, rather than parameterised (or the parameterisation significantly turned down), which may impact on the magnitude and variability of ocean heat and freshwater transports (Volkov et al. 2008; Treguier et al. 2014). Stronger sea surface temperature gradients, associated with higher ocean resolution, may improve the strength of atmosphere-ocean coupling (Brayshaw et al. 2008). Ultra-high resolution within the Agulhas region has also been shown to affect the variability of the simulated low-latitude Atlantic overturning (Biastoch et al. 2008b).

6

In this study, we document the drivers of NA SPG variability in a new, high-resolution coupled model that represents a rare combination of high resolution (in both ocean and atmosphere) and the multi-century length integration required to analyse decadal timescale modes. We ask: Does high resolution, and the associated processes it allows, affect the nature of simulated decadal variability?

The paper is structured as follows: Section 2 describes the model and data used. We then briefly characterise the model in Section 3 before exploring the mechanism of decadal variability in some depth throughout Section 4. The implications of our findings are discussed in Section 5 before conclusions in Section 6.

2. Model description and experimental setup

We examine a prototype of the Met Office Hadley Centre's state-of-the-art coupled ocean-atmosphere-land ice global environment model, HadGEM3, hereafter referred to as HG3. 460 years of near present-day control simulation have been run at high resolution. The atmosphere component is the Met Office Unified Model version 7.7 (Walters et al. 2011). It has a horizontal resolution of N216 (92km at the equator) and 85 levels in the vertical with a model top at 85km with at least 30 levels in or above the stratosphere. The ocean is resolved on the NEMO tripolar grid (0.25°, 75 depth levels, version 3.2, Madec and Coauthors (2008)), with a pole under Antarctica and poles either side of the Arctic Ocean in Asia and North America. The ocean in HG3 was initialised from rest at December 1st using the 2004–2008 time mean EN3 (Ingleby and Huddleston 2007) December-time climatology and subsequently allowed to freely evolve with repeating 2000 external forcings in the atmosphere. The year 2000 was chosen as it combined a well sampled and recorded set of external forcings with relatively neutral conditions in major cli-

7

mate indices, such as El Niño; for further details of the model configuration and other simulations see Walters et al. (2011).

We use observed data from the EN4 objective analysis (Good et al. 2013) which provides infilled, optimally interpolated fields of temperature and salinity on a $1\text{x}1^\circ$ grid from 1900 to present-day. EN4 is an updated version of EN3, with improved quality control and error estimates, but was not available when the climate model was initialised. We use the period 1900–2013 to construct a simple climatology for comparison with HG3 and note that the biases in HG3 are large enough (see Section 3a) that the method used to construct the climatology is unlikely to be of first order importance *i.e.* the results are not sensitive to choosing 1900–2013 or 1960–2013 climatologies. Unlike the HG3 model, which is run with interannually constant forcings appropriate for the year 2000, this observational data also includes the effects of all other natural and anthropogenic forcings.

HG3 is a precursor to the model used in the Met Office global seasonal forecast, GloSea5 (MacLachlan et al. 2014). GloSea5 will also be similar to the new decadal prediction model. However, there are some differences between the HG3 and GloSea5 models, as GloSea5 underwent additional development whilst the HG3 control was running. Most importantly for the present study of the NA SPG is the more diffuse thermocline in the HG3 ocean (NEMO version 3.2) as compared to GloSea5 (NEMO version 3.4, see discussion section) (Megann et al. 2014). Despite this the NA SPG biases in upper ocean temperature and salinity (compared to EN4), are small compared to many other coupled climate models used to study NA SPG variability (e.g. Escudier et al. (2013), Wang et al. (2014) (for SSTs), see Section 3a). Further details of global mean-state biases within the atmosphere and ocean in HG3 can be found in Walters et al. (2011).

3. Characterising the model

We now examine the NA mean state biases and signal of decadal variability in HG3 in some more detail as a precursor to investigating the mechanisms of variability which exist on top of these biases. In all cases, 'decadal' variability refers to 5-year smoothed data, unless otherwise stated.

a. NA SPG Mean state

Mean state biases in top 500m depth averaged temperatures (T500), salinities (S500), and densities (ρ500) in the NA SPG are less than $\pm3°C$, ±0.4PSU, and ±0.1kg/m^3 in the interior NA SPG, with larger $+4°C$, $+0.6$PSU, and ±0.2kg/m^3 biases in the boundary current regions (Figure 2). The temperature and salinity biases are close to being density compensating in the NA SPG but in the subtropical gyre (not the focus of this study) temperature biases dominate resulting in lighter waters. The anomalously cold region in the western SPG, often attributed to the simulated Gulf Stream being too zonal (Kwon et al. 2010), is not as large as in many coupled climate models (Scaife et al. 2011). Warm anomalies exist all along the NA SPG northern boundary currents. These anomalies are associated with reduced ice distribution around southern Greenland and in the Labrador Sea (not shown). Within the NA SPG, simulated deep convection, as estimated from the annual standard deviation in March mixed layer depths (using the mixed layer estimation method of Kara et al. 2000), is located in the Labrador Sea and Irminger Current.

The Atlantic meridional overturning circulation (AMOC) streamfunction in the model is shown in Figure 3a. The zero streamfunction line sits at a depth of 2–3km with the maximum overturning occurring at a depth of approximately 1km. The deeper overturning cell, representing Antarctic Bottom Water (AABW) and Lower North Atlantic Deep Water (LNADW) has a strength of around 3Sv, whereas the shallower AMOC cell, representing the western boundary current and Upper

9

North Atlantic Deep Water (UNADW) has a mean strength of 17Sv for the last 200 years of the simulation.

At 26°N it is possible to directly compare the streamfunction in the model to the RAPID observations. The depth of the RAPID overturning maximum is marked with a cross and is approximately 200m deeper than in the simulations, which at these depths represents a single model grid cell in the vertical. The depth of the RAPID zero streamfunction line is around 4km, much deeper than simulated. This is not uncommon in models and may be partly an artefact of computing the simulated overturning using the full 3-dimensional velocities (Roberts et al. 2013), although some models do represent a much deeper upper cell (Yeager and Danabasoglu 2012). Nevertheless, using a 'RAPID-style' calculation, after Roberts et al. (2013) with a depth of no motion at 4740m, yields a zero streamfunction depth approximately only 250m deeper than using the full 3-dimensional velocities. The structure and variability of the streamfunction shallower than this are essentially unchanged. Finally, the NA SPG barotropic streamfunction and associated time series are also shown (Figure 3, b and d) and broadly compare well to observational estimates and high resolution models (Tréguier et al. 2005).

Although the depth (1000m) and strength (17Sv) of the maximum of the upper AMOC cell are consistent with observations, the simulated annual variability in this index is weaker than observed. The simulated annual mean AMOC streamfunction at 26.5°N and 1000m depth has a standard deviation of 1.2Sv (0.9Sv if first detrended), compared to an annual standard deviation of 2.3Sv from the 10 years of RAPID data available (Figure 3c). Additionally, the simulated index begins at a low value and then takes several centuries to spin-up to a more stable state more favourably comparable to the observed mean. Although this represents an improvement in this index of the NA circulation, the spin-up of the overturning circulation also results in an increase

in northward heat and salt transport within the Atlantic Ocean, causing the NA SPG to drift away from its initialised state to a warmer and saltier state, seen in Figure 2

The simulated AMOC index also shows some evidence of multiannual/decadal variability, particularly at the more northerly latitudes of the NA SPG (not shown) in addition to 26N, as in other models (Zhang 2010). The maximum correlation between the simulated AMOC indices at $26.5°N$ and $50°N$ occurs when the $50°N$ index leads by 1 year (correlation of 0.63 with a correlation of 0.12 required for significance at the 95% level), suggesting the lower latitude variability is responding to variability further north in the NA SPG. We now move on to examine the decadal variability of the NA SPG in more detail.

b. Signal of decadal variability

The time-mean T500 simulated in HG3 is shown in Figure 4a along with contours at 6 and 10 degrees to mark the general shape of the NA SPG. A comparison with observations (EN4) again shows the general warm bias of the NA SPG, particularly towards the edges of the gyre. A power spectrum for T500 over the whole region reveals a significant peak at a period of 16 to 17 years (Figure 4b). This periodicity exists whether using the entire simulation or alternatively removing the first 200 years (not shown), suggesting it is not merely an adjustment process, and so we use the entire time series to maximise the available data. Additionally, the periodicity is not unique to any of the four individual subregions within the NA SPG (dashed regions in Figure 4a); all show a significant peak at 16 to 17 years, as well as the North Atlantic Current (NAC) and Irminger regions (not shown). Indeed, in HG3 many other large scale ocean indices in the NA SPG also reveal peaks in their power spectra at periods of 16 and 17 years, such as SSTs, depth averaged salinities, the AMOC at $50°N$, or the strength of the NA SPG itself (as defined by the barotropic streamfunction, *c.f.* Figure 3).

11

In addition to these ocean indices, the NAO index also shows periodicity at 16 to 17 years in its otherwise much whiter spectrum (Figure 4c). This is suggestive of a link from ocean to atmosphere in the region of the NA in which the ocean can impart some of its long term memory on to the atmosphere. Such a feedback might in general be expected to be weaker than similar atmosphere to ocean processes, and related to the strength of the ocean circulation and SST gradients (Nonaka and Xie 2003), and thus detection of this feedback is perhaps at least in part due to the increased signal to noise ratio resulting from the length of the control simulation (though we note this is still short compared to many previous studies with lower resolution models). The mechanistic drivers behind this 17 year mode in the ocean and atmosphere, and the reasons for the particular timescale, are investigated in the next sections; initially characterising the variability in the NA SPG as a whole before targeted analysis of the processes in different regions.

4. Mechanism of decadal variability in the NA SPG

We now diagnose the mechanism of decadal variability within the NA SPG, beginning with a heat budget for the region before investigating how temperature anomalies propagate around the gyre.

a. Heat budget

To begin to understand the variability of T500 in HG3 a heat budget of the NA SPG is diagnosed (Appendix). There is considerable variability in the net heat flux into the NA SPG, the majority of which appears to be attributable to the advective heat fluxes from the south, which results in decadal timescale heat content changes within the NA SPG. Annual and decadal correlations between the total heat flux and net advective fluxes are 0.75 and 0.69 (for annual and decadal data the 95% significance levels, assuming a two-tailed t-test, are 0.12 and 0.37 respectively), whereas

12

the same for the total heat flux and net surface fluxes are 0.63 and 0.29 (the regression gradients scale similarly) suggesting that particularly on decadal timescales advective heat fluxes dominate the variability. Once within the NA SPG, how do these heat content anomalies evolve?

b. Lagged regression analysis

In order to investigate the spatial characteristics of the heat content variability, lagged regressions of NA SPG T500 on to SST spatially averaged over the NA SPG were performed (Figure 5). T500 anomalies can be seen propagating around the NA SPG: eastwards along the southern boundary whilst spreading into the interior with a timescale of around 4–6 years (notably slower than implied by the mean circulation speed in this region); westwards along the northern edge but south of the Greenland, Iceland, Norwegian (GIN) Seas; into the central Labrador Sea as opposite sign anomalies form in the Gulf Stream region. A similar evolution of anomalies was also found when regressing T500 on to T500 spatial averages over the eastern SPG, NAC region, or Labrador Sea (not shown). The remaining panels will be discussed in Section 4f. Features such as the Reykjanes Ridge can be seen diverting the flow. Although not shown here, there is little evidence of significant amounts of the signal diverting into the GIN Seas in the far northern part of the SPG. The heat content anomalies reach the Labrador Sea from the eastern SPG within a couple of years but several more years are required for the anomalies to spread into the interior SPG. As the heat content anomalies in the Labrador Sea build up so does a cold anomaly in the Gulf Stream/NAC region. The opposite phase of the cycle now begins.

The underlying essence of the cycle is captured by regressing T500 indices in the northern and southern edges of the NA SPG against each other (Figure 6, the same result is also found if removing the spin-up phase, not shown). This shows the southern edge of the NA SPG leading the northern edge by 4–6 years and subsequently lagging changes in the northern edge by 0-2 years

13

with opposite sign, yielding a half period of 4–8 years and a full period of 8–16 years (constrained here to be even by the use of annual data). The timescale is further increased by 2 years (putting the 16/17 year spectral peak more towards the centre of this range) if a third location in the eastern SPG is added to the regression model, forcing the signal to go via the eastern SPG (by regressing the southern index with an index of the eastern NA SPG, and then regressing the index of the eastern NA SPG with the northern index, not shown), suggesting that the spread in timescales is perhaps related to the superposition of various advective pathways. This decadal mode is generally confined to the top 500m–1km with the exception of the central Labrador Sea where it extends to around 2km (not shown). Decadal variability in the band 10–30 years, encompassing the spectral peak at 17 years, explains >15% of the interannual variability in T500 within the NA SPG, with this value rising to >30% in the centre of the gyre.

The lagged regression analysis leads to two key questions: Firstly, what is controlling the apparent propagation of the heat content anomalies in both a) the Gulf Stream extension/NAC, and b) the northern boundary currents/Irminger Current? Secondly, what is the negative feedback which forms the opposite sign anomaly in the NAC, resulting in a cyclical mechanism and a spectral peak in NA SPG temperatures?

c. Heat content anomalies in the NAC region

To determine what controls the heat content changes on the southern boundary of the NA SPG, the heat budget of the NAC region is examined in more detail. A region was chosen where simulated zonal currents are much stronger than meridional or vertical currents (See Figure 4a, blue box). This simplifies the later interpretation of the decomposition of advective heat fluxes into circulation and temperature components. As noted in the Appendix, it is not possible to close the heat budget precisely, which becomes more apparent for smaller subregions. Table 1 shows the

14

time mean advective components and net surface heat fluxes for the NAC top 500m. Note that the choice of reference temperature becomes irrelevant when considering the net transport through all faces combined but not when considering open sections (Schauer and Beszczynska-Möller 2009). The most important advective heat fluxes are from the east and west, associated with the mean volume transport through the region from east to west. These advective heat fluxes are approximately balanced by the surface heat fluxes but the sum of the two is not identical to the actual heat content change implied by the in-situ temperatures. This is due to missing diagnostics (See Appendix) and the use of monthly means when computing vT, rather than at each model time step. However, although the means are slightly different, the variability in both time series is well correlated on all timescales at monthly or longer sampling (Table 1). Thus in the ensuing analysis of the variability we treat the budget as sufficiently closed.

The annual and decadal timescale correlations (regression gradients, W=Watts) between the advective heat fluxes and net actual heat content changes in the NAC are 0.82 (0.92 W_{dOHC}/W_{adv}) and 0.54 (0.40 W_{dOHC}/W_{adv}) respectively, compared to 0.43 (0.92 W_{dOHC}/W_{surf}) and 0.20 (0.20 W_{dOHC}/W_{surf}) for the correlation between surface heat fluxes and the net heat content change (for annual and decadal data the 95% significance levels, assuming a two-tailed t-test, are 0.12 and 0.37 respectively). Thus much of the annual and decadal variability in the heat content changes in the Gulf Stream is associated with advective heat fluxes but there is a role for surface fluxes to modulate these changes, even on decadal timescales. See Appendix 2 for the full heat transport breakdown. Of the advective heat fluxes, the remaining question is whether these are due to the anomalous circulation or anomalous temperature.

For the NAC region it can be seen that slightly more of the advective heat flux variability arises from that due to anomalous circulation advecting mean temperature anomalies ($v'T_0$, Table 3). Although the magnitudes are similar between $v'T_0$ and v_0T' components, the relationship with

15

the net ocean heat transport (OHT, *i.e.* vT) is not, with $v'T_0$ having a higher positive correlation with OHT. Correlations between $v'T_0$ and OHT are 0.29, 0.36, and 0.42 on monthly, annual, and decadal timescales respectively, compared to 0.00, -0.16, and -0.23 for v_0T' (Table 2). This holds throughout the western half of the southern edge of the NA SPG (not shown), and is associated with a strong background temperature gradient. Thus $v'T_0$ appears to be the dominant advective heat flux in the NAC region on all timescales.

d. Heat content anomalies in the Irminger Current region

The same breakdown of heat content changes into a particular region was applied to the Irminger Current at the entrance to the Labrador Sea (Figure 4a, red box). Similarly to the NAC region, this was chosen where horizontal circulation was well defined in a particular direction and much larger than all orthogonal circulations. The breakdown of heat fluxes into surface, advective, and advective subcomponents is shown in Table 1. Similarly to the Gulf Stream region, the net surface and net advective heat fluxes approximately balance but do not fully explain the directly calculated heat content change. However, as before, the correlation between the sum of the surface and advective components and the flux implied by the actual heat content change is very good on all timescales and so we again treat the budget as sufficiently closed.

For the individual fluxes, on annual timescales, the correlation (regression gradient) between the advective heat fluxes and net heat content changes is 0.56 (0.56 W_{dOHC}/W_{adv}), again marginally greater than the correlation between surface heat fluxes and net heat content changes at 0.47 (0.52 W_{dOHC}/W_{surf}). On decadal timescales these drop to 0.21 (0.08) and 0.19 (0.09) for advective and surface fluxes respectively. Despite these low decadal correlations, there is still a very large correlation between their sum and the actual net heat content change (Table 1), suggesting that on these decadal timescales no single component of the heat budget can be considered the controlling

16

influence. This is also indicated by the strong anti-correlation between advective and surface heat

fluxes of -0.87 on decadal timescales (for annual and decadal data the 95% significance levels,

assuming a two-tailed t-test, are 0.12 and 0.37 respectively).

In contrast to the Gulf Stream region, for the Irminger Current the most important advective heat

flux is that due to the mean circulation advecting anomalous temperature ($v_0 T'$, Table 3). $v_0 T'$

has slightly greater variability on all timescales than $v' T_0$ and also shows larger correlations (and

regression gradients) with the actual OHT changes on all timescales. Correlations between OHT

and $v_0 T'$ for monthly, annual, and decadal variability are 0.83, 0.34, and 0.29 respectively, whereas

correlations between OHT and $v' T_0$ are much smaller (Table 2). In our Irminger Current box the

zonal currents are an order of magnitude larger than in all other directions, and so we suggest

that it is the zonal mean circulation which is playing an important role in moving heat content

anomalies from east to west on the northern edge of the NA SPG. Additionally, the simulated

mean temperature of the core of the inflow and outflow waters differs by 0.2K in the Irminger

Current region, compared to 1.6K for the NAC region, which may help to explain the smaller

standard deviations in advective heat fluxes through the Irminger Current region.

In summary, the heat budget for the NA SPG as a whole has been diagnosed and it has been

seen that advective heat fluxes play an important role on decadal timescales, but that the relative

contributions of circulation and temperature anomalies to the OHT are region specific. We now

investigate the remaining question of what controls the negative feedback between Labrador Sea

and NAC temperature anomalies.

e. Negative feedback between Labrador Sea and Gulf Stream T500

The anomalous temperatures in the Labrador Sea, which are related to the increased heat flux

into the region, affect deep water formation in this region. As noted in Section 1, an assessment of

17

related studies suggests an approximately even split between temperature and salinity control of the Labrador Sea density changes related to increased deep water formation on decadal timescales. Following Delworth et al. (1993) we decompose the simulated density changes in the Labrador Sea into those due to temperature and those due to salinity (Figure 7a). This analysis suggests that in HG3 simulated density changes in the Labrador Sea are due to temperature induced density changes (annual correlation with actual density: 0.64, correlation required for significance at the 95% level, assuming a two-tailed t-test, is 0.12), rather than salinity induced density changes (annual correlation with actual density: -0.06). A lagged correlation analysis confirms that on both annual and decadal timescales density changes are temperature-controlled (Figure 7b). We hypothesise that simulated dense water formation in the Labrador Sea in HG3 contributes to circulation anomalies in the NAC region via the creation of an anomalous north-south dynamic height gradient, and as such acts as a negative feedback on to NA SPG temperatures.

To examine this hypothesis we calculate a composite difference in the density in a cross section through the NAC which lags the density upstream in the Labrador Sea (Figure 8a). To the north the connection between surface and deep water is revealed with the signal sinking below the surface as it progresses southwards. The north-south density gradient is associated with a change in the local dynamic height (Figure 8b). Despite the negative density anomaly in the south it can be seen that a large part of the dynamic height anomaly is controlled by the northern, positive density anomaly.

As the signal of anomalous density spills out of the Labrador Sea this dynamic height gradient increases and is balanced by anomalous shear in the geostrophic velocities (Figure 8c). The mean geostrophic velocity anomaly between the surface and 500m for the pictured transect is 1.2cm/s, increasing to 1.6cm/s for the top 200m only. Thus, an increase in density in the Labrador Sea, associated with a cooling in this region, is followed by a strengthening of the circulation in the NAC, and thus an increase in northward OHT into the NA SPG (with likely also some additional

18

contribution from $v'T'$ as the anomalous circulation acts on anomalously warm, low density surface water, *c.f.* Figure 8a). This acts as a negative feedback on the NA SPG temperatures. We now discuss the atmospheric contribution to these ocean feedbacks.

f. The role of the atmosphere

Although the proposed mechanism of decadal (17 year) variability in HG3 has been described mostly in terms of ocean dynamics there are regions where the atmosphere directly forces, or acts as a positive feedback on, the ocean variability.

For example, the negative feedback dipole between Labrador Sea and NAC temperatures is reminiscent of the Ekman response to NAO forcing. To quantify the instantaneous (*i.e.* zero lag) impact of the NAO we attempt to isolate its signal similarly to the analysis of Polo et al. (2014). Specifically, the annual mean 3-dimensional ocean density field was regressed onto the wintertime NAO index (both unfiltered, not shown). The direct impact of the NAO was then removed from the density field by scaling the regression pattern by the NAO index and removing the pattern from the density at each time point. Removing the instantaneous NAO-related signal weakens the density/dynamic height and thus geostrophic current response (Figure 8d) calculated in Section 4e, hence suggesting that some of the proposed ocean negative feedback is forced by the atmosphere and not merely an ocean-only process. On annual timescales the magnitude of the current response is reduced by 45% but on longer, decadal timescales the reduction is less stark (13% reduction, shown in Figure 8d). This analysis assumes that the instantaneous impact of the NAO is annually independent and can be linearly separated. To what extent the NAO and ocean temperatures/densities can be seen as one-way forcing from atmosphere to ocean, and to what extent it is actually a coupled feedback (*i.e.* some of the NAO signal is itself forced by the ocean, implied by the spectral peak in the NAO power spectrum Figure 4c), is discussed below.

19

However, the reduction in anomalous circulation response when removing the NAO suggests that atmospheric forcing/the NAO may act to reinforce this ocean feedback.

In the northern NA SPG we have previously shown a role for ocean advection in moving heat content anomalies westwards via the mean circulation (Section 4d). At the same time, surface heat fluxes were also shown to be non-negligible. In Figure 5 the SST, T500 (discussed in Section 4b), SHF, Sea Surface Salinity (SSS), Mean Sea Level Pressure (MSLP), and Sea ice are regressed at various lags against NA SPG mean SSTs. The SHF is directed into the ocean and at lag=0,+2 is having a cooling effect in the eastern SPG and a warming effect in the western SPG, *i.e.* it is effectively moving heat content anomalies from east to west. This is likely related to the concomitant strongly negative NAO anomaly in the MSLP field at the same lags. The actual magnitude of the SHF contribution to the Irminger Current OHC change is similar to the contribution from advective fluxes (Table 1) but, as noted in Section 4d, both are individually quite poorly correlated with the OHC change on multiannual timescales. This is consistent with a mechanism whereby the ocean integrates up the interannually independent forcing from the atmosphere/NAO resulting in decadal timescale variability in ocean heat content. However, the spectral peak in the NAO index (Figure 4c) also implies some ocean to atmosphere forcing.

Additionally, in the eastern SPG, the SSTs are anti-correlated with the NAO index, seen both at the lag=0 regression and with the opposite phase at lag=-6. These SSTs are likely a combination of the direct forcing of both 1) the NAO via SHFs and anomalous Ekman and gyre circulation (Hakkinen and Rhines 2004; Sarafanov et al. 2008) and 2) the advective heat flux associated with the diagnosed mechanism of decadal variability. As noted previously, the simulated NAO shows a spectral peak at 17 years similarly to ocean indices within the NA SPG. It would appear most likely that this atmospheric memory must come from the ocean but unfortunately long enough atmosphere-only experiments with this model are not available to further test this hypothesis.

At lag=0 (and with opposite phase at lag=-6), the anomalous NAO-related SHFs show the same sign change over both the Labrador Sea and Gulf Stream/NAC but over the Gulf Stream/NAC they are of the wrong sign to explain the heat content changes (both at the surface and throughout at least the top 500m of the water column). This is consistent with advective heat fluxes playing a much more dominant role in the heat budget of the NAC region (see Section 4c) than the Irminger Current/Labrador Sea region (Section 4d). However, as noted at the beginning of this section, in the NAC region there is a significant portion of the ocean geostrophic circulation (and associated heat transport) response which is itself related to the NAO (*c.f.* Figures 8c and 8d). In short, it is impossible to completely separate the effects of either the atmosphere or ocean.

SSS evolves similarly to SST in the NA SPG although the largest changes are associated with movement of the ice edge in the GIN Seas (Figure 5; first, fourth, and sixth columns). In general in the NA SPG, positive salinity anomalies co-vary with positive temperature anomalies in both space and time, again suggesting a role for advective fluxes. NAO-related surface freshwater fluxes are also proposed to be of only secondary importance due to the fact that simulated SSS anomaly magnitudes are independent of the amplitude of the NAO (not shown).

Similarly to other large scale variables within the NA SPG, ice edge changes exhibit decadal variability with a spectral peak at a period of 17 years (not shown). However, unlike in similar work with the IPSL model (Escudier et al. 2013) negative sea ice anomalies do not appear to lead cooling in the NA SPG (Figure 5, sixth column). We suggest that in our simulations ice edge changes are primarily a passive response to the temperature dominated decadal variability within the NA SPG, perhaps again via the NAO (Deser et al. 2000), rather than a direct driver of this variability.

g. Summary of the proposed mechanism

The mechanism of decadal (17 year) variability simulated in the NA SPG T500 and SSTs is summarised in Figure 9. Positive circulation anomalies in the southern part of the SPG move heat eastwards and northwards into the eastern SPG with a timescale of around 5 years (orange). These heat content anomalies are then transported by the mean circulation around the northern edge of the SPG with a timescale of around 2 years (red). In the Labrador Sea these anomalies affect the stability of the water column. These negative density anomalies, associated with reduced deep water formation, spill out from the Labrador Sea into the SPG, deepening as they go. In the region north of the Gulf Stream these negative density anomalies affect the north-south density gradient and induce geostrophic circulation anomalies weakening the NAC. The weaker circulation reduces ocean heat transport and acts to cool the NA SPG (blue). The phase of the oscillation is thus reversed.

The postulated role of the atmosphere is also noted (black dashed lines in Figure 9): As temperature anomalies build up in the eastern SPG the atmosphere acts to strengthen these anomalies. When the east of the NA SPG is anomalously warm or cold SHFs also act to move the ocean heat content anomaly westwards. Lastly, in the region of the Labrador Sea/Gulf Stream temperature (density) dipole the NAO is associated with around 13% of the ocean-circulation feedback (calculated in Section 4e and shown in Figure 8d).

We now discuss the implications of our work and similarities between it and previous studies.

5. Discussion

In the context of the brief literature summary in Section 1, and the schematic illustration presented in Figure 1, our simulations broadly fall into a temperature-dominated regime in the Labrador Sea in which the mechanism could be described as 'Ocean*' (where the asterisk implies

a positive feedback between the NAO and SSTs may be amplifying the mode, after Figure 1). The timescale is set in part by mean circulation speeds in the northern SPG but with a transition to anomalous circulation in the southern SPG — although it is not clear from the simulations precisely where this transition occurs.

The simulated timescales between changes in the Labrador Sea, NAC and eastern SPG have been attributed to advective processes. However, confounding this are wave processes which are also weakly detectable within the model. Analysis of the deep density field (1500–3000m, not shown) reveals signals characteristic of boundary waves propagating from the Labrador Sea to the equator; propagating along the equator to the eastern boundary; subsequently propagating north and south along the eastern boundary, all the while radiating Rossby waves westwards. The evolution is very similar to that found in the idealised model of Johnson and Marshall (2002) and yield a lag between the Labrador Sea and eastern SPG of 5 years, broadly similar to that due to advection. Although detectable, these wave signals require heavy filtering of the deep density field whilst the proposed mechanism exists mainly in the top 1km. We can only conclude that wave processes may play an additional role in our simulated variability but the magnitude of this is unclear. We also note that the relatively diffuse thermocline in HG3 (Megann et al. 2014) may act to dampen these wave processes (Grotzner et al. 1998) as compared to the updated seasonal forecast model, GloSea5 (which will be similar to the new Met Office decadal prediction model).

Despite the lagged regression analysis used in this study, and its ubiquity within studies of decadal variability within climate models, there are some hints from the present work that the proposed mechanism may be asymmetric. This asymmetry is manifest in the timescales of various phases of the cycle being also dependant on the sign of the anomaly; *i.e.* the same processes are at work in opposite phases of the mechanism but may evolve with different timescales. Some evidence for this can be seen in Figure 5 in which all the fields reverse sign over 6–8 years,

23

implying a periodicity of 12–16 years, and yet the spectral peak occurs at the upper end of this at 16 to 17 years. If we construct lagged composites of the T500 (or SST) field based on the top/bottom 10% of phases of the SST index (not shown) we find a reversal timescale of 10 years following a high SST phase, but a reversal time of 6 years following a low SST phase. This asymmetrical timescale doesn't appear to be directly due to the effect of heat transport by the anomalous circulation in the southern SPG ($v'T_0$, see Section 4c) as the lags between the NAC and eastern SPG are the same timescale in both phases. It is important to note though that constructing composites, which only use 20% of the total data, reduces the number of degrees of freedom.

This asymmetry also appears evident in the coupled simulation when compositing MSLP based on high/low phases of the SST index. Although both MSLP patterns, composited against positive SSTs (Figure 10a) and negative SSTs (Figure 10b), show significant MSLP anomalies, the magnitude and precise structure are clearly different, with only the negative SST composite associated with the canonical NAO pattern (Figure 10b). Additionally, atmosphere-only sensitivity experiments (not shown) suggest a stronger coupling in the NA SPG between anomalously positive NAO/negative SSTs than anomalously negative NAO/positive SSTs. We plan to investigate the asymmetry further in a separate study.

Comparison with observations and other models

It is difficult to that the prove the mode of variability reported here is inconsistent with observational data due to the paucity of observational records in the NA SPG, particularly in the northern half, and the presence of confounding additional transient forcings in the observational record. However, palaeo proxies from the NA SPG suggest there is 20 year variability in some indices in the region (Sicre et al. 2008; Chylek et al. 2012), although it must be noted that there is disagreement on the spectral characteristics of all proxies (Mann et al. 1995). The specific elements

of our proposed mechanism (anomalous circulation OHT in the southern part of the NA SPG, mean circulation OHT in the northern part, a negative feedback between Labrador Sea and NAC temperatures) are also broadly consistent with the observational literature. For example, there are some similarities to the anti-correlated relationship between Labrador Sea and NAC temperatures/transports seen in observations (Curry and McCartney 2001). This observational work also highlights the significant role of the NAO in this relationship as well as the dominant role for temperature (as opposed to salinity) in driving these changes. We note that as a result of the northern NA SPG warm bias in HG3 there is less ice in the mean, which may detrimentally affect the ability of ice/freshwater fluxes to affect the decadal variability. In models where the NA SPG mean state bias is cold, feedbacks involving ice and freshwater fluxes have been shown to be crucial to the diagnosed decadal variability (Escudier et al. 2013).

Although it is difficult to isolate the precise mechanisms by which increased ocean or atmosphere resolution may have altered our results — without a parallel set of low resolution simulations within the same model framework — there are specific features of the decadal variability that are likely to be affected by enhanced resolution. For example, our proposed mechanism of NA SPG decadal variability suggests a prominent role for boundary currents, which may be improved by higher resolution (Grotzner et al. 1998; Gelderloos et al. 2011). Additionally, the increased atmospheric resolution (which represents the main computational burden for the coupled model) may affect the innate atmospheric variability over the North Atlantic (Matsueda et al. 2009), while the role of the atmosphere may also be modulated by the improved ocean resolution (Scaife et al. 2011). Recent work comparing $1°$, $0.25°$, and $^1/_{12}°$ resolution simulations with the same underlying model suggest that $0.25°$ is a significant improvement over $1°$, in terms of the biases in NA SPG SSTs and the location of the Gulf Stream, but that there are still further improvements to be had at even higher resolution (Marzocchi et al. 2015).

Similar to our findings, recent ultra-high resolution ($^1/_{12}$° horizontal resolution) eddy resolving ocean-only model studies show that much of the OHT into the eastern NA SPG occurs in the near surface (but below the Ekman layer) originating in the subtropics (25% of virtual floats at 500m, compared to less than 10% at 50m or 1000m (Burkholder and Lozier 2011, 2014)). In addition, the role of anomalous circulation transporting the mean temperature gradient in the southern part of the NA SPG is indirectly supported by these ocean-only simulations, which find that the mean circulation is unable to explain the slow timescale by which temperature anomalies move from the subtropics to the eastern SPG. Important for decadal variability in our simulations are advective heat fluxes from the southern edge of the NA SPG due to the anomalous circulation ($v'T_0$). However, annual variability (*i.e.* the anomaly) in the AMOC at 26.5°N from 10 years of RAPID data is approximately double the annual standard deviation in HG3. Thus, if the proposed mechanism exists in reality then it could be expected to have a larger amplitude or faster timescale.

The mechanism we have presented has a timescale of 17 years, similar to the 20 years found in the IPSL-CM5A-LR model recently investigated by Escudier et al. (2013). However, a similar timescale does not imply the same mechanism: see for example an identical 17 year timescale but different mechanism reported by Born and Mignot (2012). The present study reports a mode of variability where temperature dominates the density budget, whereas Escudier et al. (2013) report a mode in which freshwater/salinity fluxes have an important role. Indeed, salinity advection within the SPG has been proposed as a cause of bistability in the SPG (Born et al. 2013), albeit on longer timescales. It is intuitive that whether the density budget is dominated by temperature or salinity would affect whether a strengthening northward circulation acted as a positive or negative feedback — but why are NA SPG density changes differently controlled in the two models?

One hypothesis is that the nature of the biases (compared to observations) affects the variability as the non-linear equation of state for density becomes increasingly salinity dominated at cooler

26

temperatures. To estimate this effect we compute the density change in the Irminger Current region, mechanistically important in both studies, for a one standard deviation change in temperature or salinity (whilst keeping the other of salinity or temperature at climatological values) in both HG3 and the IPSL-CM5A-LR model as well as an observational estimate from EN4 (Table 4). In HG3, such a temperature change has double the impact on density than a change in salinity. This is not the case in the IPSL model where salinity changes are found to be more important (the relative magnitudes are unchanged if we remove the spin-up in HG3, not shown). The EN4 data suggest that the real world may be in a temperature dominated regime, similar to HG3. This points to there being some relationship between the NA SPG mean state biases of a given model and the subsequently diagnosed mechanisms of decadal variability. Note that this cursory analysis merely compares mean states and variability, and does not explicitly investigate whether density variability is temperature- or salinity-controlled. Nevertheless, one implication of this would be that decadal prediction studies using anomaly-assimilation methods, in which the mean state biases are implicitly assumed to be independent of the variability, would need to re-evaluate the validity of this assumption (Robson 2010). We plan to investigate this relationship in more detail in a forthcoming study (Menary et al. 2015).

6. Conclusions

We have analysed a decadal mode of variability in the near surface (top 500m) of the North Atlantic subpolar gyre (NA SPG) in a 460 year control simulation with a version of the high resolution coupled climate model HadGEM3 (HG3).

- The mode of variability involves the propagation of heat content anomalies around the NA SPG with a periodicity of around 17 years.

27

- Simulated decadal variability (between 10 to 30 years) in the NA SPG explains more than 15% of the annual mean variance in top 500m depth averaged temperatures. This rises to >30% of the variance within the interior NA SPG and Labrador Sea.

- The simulated NA SPG heat budget is dominated by advective, rather than surface, heat fluxes on decadal timescales, with advection from the subtropics playing the primary role. For the specific regions of interest, namely the Irminger Current and North Atlantic Current (NAC), advective fluxes were also found to dominate. The large depth extent of the mode is also consistent with an important role for advection (Saravanan and McWilliams 1998).

- The role of mean or anomalous circulation in transporting heat content anomalies was found to vary with region: Anomalous circulation dominated the variability in the NAC with mean circulation, and hence temperature anomalies, dominant in the Irminger Current region.

- A negative feedback, required for the mechanism to result in a spectral peak, occurs between the Labrador Sea and NAC. Here, density anomalies spill out of the Labrador Sea resulting in a dynamic height gradient across the NAC/Labrador Sea which induces vertical shear in the geostrophic currents. These current anomalies result in heat transport anomalies which reverse the cycle. The density changes are temperature, rather than salinity, driven.

- Variability in the NAO directly contributes to various stages of the mechanism as well as showing signs of responding to ocean variability. Removing the North Atlantic Oscillation (NAO) signal from the negative feedback between Labrador Sea and NAC temperatures/densities (see Section 4f) shows about 45% of the geostrophic current speed feedback is related to the NAO on annual timescales but that on decadal timescales the ocean feedback still dominates. The atmosphere also acts to reinforce temperature anomalies in the eastern

28

NA SPG and aid their westward propagation in the northern SPG. The proposed mechanism is summarised in Figure 9.

- Whether density changes are temperature or salinity controlled effects where, and how, negative feedbacks can occur. This may also be expected to affect the particular mechanism simulated in the model. This could have important implications for decadal prediction studies that use the method of anomaly-assimilation and prediction, in which the future evolution of the model is assumed to be independent of the mean state — an assumption which we suggest may not be valid.

A modified version of the model presented here will be used as part of the Met Office decadal prediction system and analyses such as we have presented will be important in developing and evaluating such systems. Given the relationship between resolution and the improved realisation of particular processes, as well as mean state biases, further high resolution coupled model studies would be valuable in testing whether these results are robust.

APPENDIX

Heat budget

The basin-wide, full depth NA SPG heat budget is shown in Figure 11 for the latitude range 53–73°N. Due to the lack of availability of the correct ocean diagnostics at high enough output frequency (precluded by the expense of storing high resolution atmosphere and ocean data), the heat budget of the NA SPG does not close perfectly (*c.f.* red and black lines in Figure 11a). However, the error is negligible, less than 1% of the net surface fluxes of the region. Sensitivity tests where all output diagnostics were computed online and stored revealed that horizontal diffusion was the most important missing heat flux. The heat budget of the NEMO ocean is further complicated by the use of a linear free surface with variable volume which sits on top of the fixed volume ocean grid cells and a heat flux between the two. For further details of the precise formulation of the heat budget within the NEMO ocean model see Madec and Coauthors (2008).

The heat budget (ocean heat content (OHC) rate of change) of the NA SPG can first be broken down into advective (Q_{adv}) and surface fluxes (Q_{surf}), which add together to give the net heat flux *into* the volume. There are also additional smaller heat fluxes from the ice to ocean, between the linear free surface and fixed ocean volume, and from geothermal heating of the abyssal ocean, particularly in the vicinity of the mid Atlantic ridge, Q_{ice}, Q_{free}, and Q_{geo} respectively:

$$\frac{\mathrm{d}OHC}{\mathrm{d}t} = Q_{adv} + Q_{surf} + Q_{ice} + Q_{free} + Q_{geo} \tag{A1}$$

The advective fluxes can be further broken down into fluxes from the north ($OHTN$) and south ($OHTS$, positive northward) whilst the surface fluxes can be broken down into the shortwave (solar), longwave, latent, and sensible heat fluxes:

$$Q_{adv} = OHTS - OHTN \qquad (A2)$$

$$Q_{surf} = Q_{SW} + Q_{LW} + Q_{lat} + Q_{sens} \qquad (A3)$$

This reveals that $OHTS$ dominates the variability in advective heat fluxes: Using annual data, the standard deviation of $OHTS$ is 28PW, compared to 17PW for $OHTN$. The variability in $OHTS$ is split between vertical 'AMOC' and horizontal 'gyre' heat transport variability at these latitudes (annual correlation between $OHTS$ and OHT_{AMOC} is 0.74, and between $OHTS$ and OHT_{gyre} is 0.88). The surface fluxes (directed into the ocean) are dominated by shortwave (solar) heating of the NA SPG, whereas longwave, latent, and sensible heat fluxes represent net heat loss from the NA SPG.

To investigate the relative magnitudes of their variability, and any trends, the mean of each heat flux over the years 22–42 is removed (Figure 11b). Rather than remove the full time mean, removing the mean from just the period soon after the model was initialised serves to additionally show how the heat fluxes diverge. Net advective heat fluxes into the region are increasing throughout the period, balanced largely by increasing surface heat flux loss, but with some residual heating of the NA SPG. The advective heat flux trend is dominated by the increase in heat flux from the south, which is due to the strengthening AMOC (Figure 3c), with much of this heat lost via latent heat loss as well as longwave emission. The rate of net warming is highest in the first century, which is also why the net heat flux appears to be below zero for the remainder of the time, *i.e.* the net warming rate is slower in the subsequent years.

APPENDIX 2

Heat budget breakdown

31

Previously Dong and Sutton (2001), showed the advective heat budget for a region in approximate long term equilibrium could be estimated by considering perturbations around a long term mean as:

$$q(t) = \bar{q} + q'(t) \tag{21}$$

where $q(t)$ is some quantity varying in time, $\bar{q}$ is its time mean, and $q'(t)$ is the anomaly in q at each time, t. For the case of the net advective heat transport convergence, replacing q with both v (velocity) and T (temperature) and dropping the (t) on the right hand side for clarity gives:

$$OHT(t) = \rho \times c_p \times \int \left(\bar{v}\bar{T} + v'T' + \bar{v}T' + v'\bar{T} \right) \mathrm{d}A \tag{22}$$

where ρ is density, c_p is the heat capacity of sea water, $\bar{v}\bar{T}$ is a constant (the mean heat transport when multiplied by ρc_p), $v'T'$ is the heat transport due to co-variances in circulation and temperature (and is usually but not always small for large enough areas), $\bar{v}T'$ is the heat transport by the mean circulation, $v'\bar{T}$ is the heat transport by the anomalous circulation, and $\mathrm{d}A$ indicates integrating over all faces enclosing the volume. vT is estimated at horizontal and vertical faces.

However, as previously mentioned, there is a trend in the NA SPG temperatures, and so the breakdown of the heat budget is made more complicated. For the case of a known trend in one or more of these parameters (*e.g.* temperature) the q' term will not just represent the annual/decadal anomaly but will also have a component due to the trend with the relative contributions to q' varying in size depending on the magnitude of the trend compared to the magnitude of the variability. Thus q must be detrended prior to combining the terms together, *e.g.*

$$q(t) = q_0 + q_1 \times t + q'(t) \tag{23}$$

32

where q_0 is the intercept, q_1 is the linear trend multiplied by time, t, and q' is the perturbation from this trend. Setting $t = 0$ at the mid point of the linearly trending time series results in q_0 also representing the mean (previously $\bar{q}$). This results in the OHT becoming an equation of nine terms (as we detrend v as well due to the trend in the AMOC, Figure 3c):

$$OHT(t) = \rho \times c_p \times \int \Big(v_0 T_0 + v_0 T_1 t + v_0 T' + v_1 t T_0$$
$$+ v_1 T_1 t^2 + v_1 t T' + v' T_0 + v' T_1 t + v' T' \Big) \mathrm{d}A \quad (24)$$

where the terms inside the integral on the right hand side respectively refer to: 1) The time mean OHT, 2) the interaction between the temperature trend and the mean circulation, 3) the OHT by the mean circulation, 4) the interaction between the mean temperature and the trend in circulation, 5) the interaction between the trends in both circulation and temperature, 6) the interaction between the trend in circulation and the anomalous temperatures, 7) the OHT by the anomalous circulation, 8) the interaction between the anomalous circulation and the trend in temperatures, and 9) the OHT due to co-variances in circulation and temperature. Analysis of these components reveals a non-zero contribution from trend-related terms to the advective heat budget variability, but this is much smaller than the mean and anomalous circulation terms ($v_0 T'$ and $v' T_0$) and as so we focus on these latter circulation terms.

References

Alvarez-Garcia, F., M. Latif, and A. Biastoch, 2008: On multidecadal and quasi-decadal north atlantic variability. *Journal of Climate*, **21 (14)**, 3433–3452.

Battisti, D., U. Bhatt, and M. Alexander, 1995: A modeling study of the interannual variability in the wintertime North Atlantic Ocean. *Journal Of Climate*, **8 (12)**, 3067–3083, doi:{10.1175/

1520-0442(1995)008\textless3067:AMSOTI\textgreater2.0.CO;2}.

Biastoch, A., C. W. Boening, J. Getzlaff, J.-M. Molines, and G. Madec, 2008a: Causes of interannual-decadal variability in the meridional overturning circulation of the midlatitude north atlantic ocean. *Journal Of Climate*, **21 (24)**, 6599–6615, doi:{10.1175/2008JCLI2404.1}.

Biastoch, A., C. W. Boening, and J. R. E. Lutjeharms, 2008b: Agulhas leakage dynamics affects decadal variability in Atlantic overturning circulation. *Nature*, **456 (7221)**, 489–492, doi:{10. 1038/nature07426}.

Born, A., and J. Mignot, 2012: Dynamics of decadal variability in the atlantic subpolar gyre: a stochastically forced oscillator. *Climate dynamics*, **39 (1-2)**, 461–474.

Born, A., T. F. Stocker, C. C. Raible, and A. Levermann, 2013: Is the atlantic subpolar gyre bistable in comprehensive coupled climate models? *Climate dynamics*, **40 (11-12)**, 2993–3007.

Brayshaw, D. J., B. Hoskins, and M. Blackburn, 2008: The storm-track response to idealized sst perturbations in an aquaplanet gcm. *Journal of the Atmospheric Sciences*, **65 (9)**, 2842–2860.

Burkholder, K. C., and M. S. Lozier, 2011: Mid-depth lagrangian pathways in the north atlantic and their impact on the salinity of the eastern subpolar gyre. *Deep Sea Research Part I: Oceano-graphic Research Papers*, **58 (12)**, 1196 – 1204, doi:http://dx.doi.org/10.1016/j.dsr.2011.08.007, URL http://www.sciencedirect.com/science/article/pii/S09670637110%01531.

Burkholder, K. C., and M. S. Lozier, 2014: Tracing the pathways of the upper limb of the north atlantic meridional overturning circulation. *Geophysical Research Letters*, **41 (12)**, 4254–4260.

Cabanes, C., T. Lee, and L.-L. Fu, 2008: Mechanisms of interannual variations of the meridional overturning circulation of the North Atlantic Ocean. *Journal Of Physical Oceanography*, **38 (2)**, 467–480, doi:{10.1175/2007JPO3726.1}.

Chylek, P., C. Folland, L. Frankcombe, H. Dijkstra, G. Lesins, and M. Dubey, 2012: Greenland ice core evidence for spatial and temporal variability of the atlantic multidecadal oscillation. *Geophysical Research Letters*, **39 (9)**.

Curry, R., and M. McCartney, 2001: Ocean gyre circulation changes associated with the North Atlantic Oscillation. *Journal Of Physical Oceanography*, **31 (12)**, 3374–3400, doi:{10.1175/ 1520-0485(2001)031\textless3374:OGCCAW\textgreater2.0.CO;2}.

Dai, A., A. Hu, G. Meehl, W. Washington, and W. Strand, 2005: Atlantic thermohaline circulation in a coupled general circulation model: Unforced variations versus forced changes. *Journal Of Climate*, **18 (16)**, 3270–3293, doi:{10.1175/JCLI3481.1}.

Danabasoglu, G., 2008: On Multidecadal Variability of the Atlantic Meridional Overturning Circulation in the Community Climate System Model Version 3. *Journal Of Climate*, **21 (21)**, 5524–5544, doi:{10.1175/2008JCLI2019.1}.

Delworth, T., S. Manabe, and R. Stouffer, 1993: Interdecadal variations of the thermohaline circulation in a coupled ocean-atmosphere model. *Journal Of Climate*, **6 (11)**, 1993–2011, doi: {10.1175/1520-0442(1993)006\textless1993:IVOTTC\textgreater2.0.CO;2}.

Deser, C., J. E. Walsh, and M. S. Timlin, 2000: Arctic sea ice variability in the context of recent atmospheric circulation trends. *J. Climate*, **13 (3)**, 617–633, doi:doi:10. 1175/1520-0442(2000)013\textless0617:ASIVIT\textgreater2.0.CO;2, URL http://dx.doi.org/ 10.1175/1520-0442(2000)013"textless0617:ASI%VIT"textgreater2.0.CO;2.

Deshayes, J., R. Curry, and R. Msadek, 2014: Cmip5 model intercomparison of freshwater budget and circulation in the north atlantic. *Journal of Climate*, **27 (9)**, 3298–3317.

Dong, B., and R. Sutton, 2001: The dominant mechanisms of variability in Atlantic ocean heat transport in a coupled ocean-atmosphere GCM. *Geophysical Research Letters*, **28 (12)**, 2445–2448, doi:{10.1029/2000GL012531}.

Dong, B., and R. Sutton, 2005: Mechanism of interdecadal thermohaline circulation variability in a coupled ocean-atmosphere GCM. *Journal Of Climate*, **18 (8)**, 1117–1135.

Dunstone, N., D. Smith, and R. Eade, 2011: Multi-year predictability of the tropical atlantic atmosphere driven by the high latitude north atlantic ocean. *Geophysical Research Letters*, **38 (14)**.

Eden, C., and R. J. Greatbatch, 2003: A damped decadal oscillation in the north atlantic climate system. *Journal of climate*, **16 (24)**, 4043–4060.

Eden, C., and J. Willebrand, 2001: Mechanism of interannual to decadal variability of the North Atlantic circulation. *Journal Of Climate*, **14 (10)**, 2266–2280, doi:{10.1175/1520-0442(2001) 014\textless2266:MOITDV\textgreater2.0.CO;2}.

Escudier, R., J. Mignot, and D. Swingedouw, 2013: A 20-year coupled ocean-sea ice-atmosphere variability mode in the north atlantic in an AOGCM. *Climate dynamics*, **40 (3-4)**, 619–636.

Fevrier, S., J. Sirven, and C. Herbaut, 2007: Interaction of a coastal kelvin wave with the mean state in the gulf stream separation area. *Journal Of Physical Oceanography*, **37 (6)**, 1429–1444, doi:{10.1175/JPO3062.1}.

Folland, C., T. Palmer, and D. Parker, 1986: Sahel rainfall and worldwide sea temperatures, 1901–85. *Nature*, **320 (6063)**, 602–607.

Frankcombe, L. M., A. von der Heydt, and H. A. Dijkstra, 2010: North atlantic multidecadal climate variability: An investigation of dominant time scales and processes. *Journal Of Climate*, **23 (13)**, 3626–3638, doi:{10.1175/2010JCLI3471.1}.

36

Frankignoul, C., P. Muller, and E. Zorita, 1997: A simple model of the decadal response of the ocean to stochastic wind forcing. *Journal Of Physical Oceanography*, **27 (8)**, 1533–1546, doi: {10.1175/1520-0485(1997)027\textless1533:ASMOTD\textgreater2.0.CO;2}.

Gelderloos, R., C. A. Katsman, and S. S. Drijfhout, 2011: Assessing the roles of three eddy types in restratifying the labrador sea after deep convection. *Journal of Physical Oceanography*, **41 (11)**, 2102–2119.

Goldenberg, S. B., C. W. Landsea, A. M. Mestas-Nuez, and W. M. Gray, 2001: The recent increase in atlantic hurricane activity: Causes and implications. *Science*, **293 (5529)**, 474–479, doi:10. 1126/science.1060040, URL http://www.sciencemag.org/content/293/5529/474.abstract, http:// www.sciencemag.org/content/293/5529/474.full.pdf.

Good, S. A., M. J. Martin, and N. A. Rayner, 2013: En4: Quality controlled ocean temperature and salinity profiles and monthly objective analyses with uncertainty estimates. *Journal of Geophysical Research: Oceans*, **118 (12)**, 6704–6716.

Grotzner, A., M. Latif, and T. Barnett, 1998: A decadal climate cycle in the north atlantic ocean as simulated by the ECHO coupled GCM. *Journal Of Climate*, **11 (5)**, 831–847, doi:{10.1175/ 1520-0442(1998)011\textless0831:ADCCIT\textgreater2.0.CO;2}.

Hakkinen, S., and P. B. Rhines, 2004: Decline of subpolar north atlantic circulation during the 1990s. *Science*, **304 (5670)**, 555–559, doi:10.1126/science.1094917, URL http://www. sciencemag.org/content/304/5670/555.abstract, http://www.sciencemag.org/content/304/5670/ 555.full.pdf.

Hodson, D. L., and R. T. Sutton, 2012: The impact of resolution on the adjustment and decadal variability of the atlantic meridional overturning circulation in a coupled climate model. *Climate*

dynamics, **39 (12)**, 3057–3073.

Holland, M., C. Bitz, M. Eby, and A. Weaver, 2001: The role of ice-ocean interactions in the variability of the North Atlantic thermohaline circulation. *Journal Of Climate*, **14 (5)**, 656–675, doi:{10.1175/1520-0442(2001)014\textless0656:TROIOI\textgreater2.0.CO;2}.

Ingleby, B., and M. Huddleston, 2007: Quality control of ocean temperature and salinity profiles. historical and real-time data. *Journal of Marine Systems*, **65 (1)**, 158–175.

Johnson, H., and D. Marshall, 2002: Localization of abrupt change in the North Atlantic thermohaline circulation. *Geophysical Research Letters*, **29 (6)**, doi:{10.1029/2001GL014140}.

Jungclaus, J., H. Haak, M. Latif, and U. Mikolajewicz, 2005: Arctic-North Atlantic interactions and multidecadal variability of the meridional overturning circulation. *Journal Of Climate*, **18 (19)**, 4013–4031.

Kara, A., P. Rochford, and H. Hurlburt, 2000: An optimal definition for ocean mixed layer depth. *Journal Of Geophysical Research-Oceans*, **105 (C7)**, 16 803–16 821, doi:{10.1029/2000JC900072}.

Kleppin, H., M. Jochum, B. Otto-Bliesner, C. A. Shields, and S. Yeager, 2015: Stochastic atmospheric forcing as trigger for sudden greenland warmings. *Journal of Climate (submitted)*.

Knight, J., R. Allan, C. Folland, M. Vellinga, and M. Mann, 2005: A signature of persistent natural thermohaline circulation cycles in observed climate. *Geophysical Research Letters*, **32 (20)**, doi:{10.1029/2005GL024233}.

Kwon, Y.-O., M. A. Alexander, N. A. Bond, C. Frankignoul, H. Nakamura, B. Qiu, and L. A. Thompson, 2010: Role of the gulf stream and kuroshio-oyashio systems in large-scale atmosphere-ocean interaction: A review. *Journal of Climate*, **23 (12)**, 3249–3281.

Kwon, Y.-O., and C. Frankignoul, 2014: Mechanisms of multidecadal atlantic meridional over-turning circulation variability diagnosed in depth versus density space. *Journal of Climate*, **27 (24)**, 9359–9376.

MacLachlan, C., and Coauthors, 2014: Global seasonal forecast system version 5 (glosea5): a high resolution seasonal forecast system. *Quarterly Journal of the Royal Meteorological Society*.

MacMartin, D. G., E. Tziperman, and L. Zanna, 2013: Frequency domain multimodel analysis of the response of atlantic meridional overturning circulation to surface forcing. *Journal of Climate*, **26 (21)**, 8323–8340.

Madec, G., and Coauthors, 2008: Nemo ocean engine: Note du pole de modélisation, institut pierre-simon laplace (ipsl), france, no 27 issn no 1288-1619, available at: http://www.nemo-ocean.eu. Tech. rep., IPSL LSCE, UVSQ, CEA CNRS, Unite Mixte, Bat 712, F-91191 Gif Sur Yvette, France.

Mann, M., J. Park, and R. Bradley, 1995: Global Interdecadal And Century-Scale Climate Oscil-lations During The Past 5 Centuries. *Nature*, **378 (6554)**, 266–270, doi:{10.1038/378266a0}.

Marzocchi, A., J. J.-M. Hirschi, N. P. Holliday, S. A. Cunningham, A. T. Blaker, and A. C. Coward, 2015: The north atlantic subpolar circulation in an eddy-resolving global ocean model. *Journal of Marine Systems*, **142 (0)**, 126 – 143, doi:http://dx.doi.org/10.1016/j.jmarsys.2014.10.007, URL http://www.sciencedirect.com/science/article/pii/S09247963140%02437.

Matsueda, M., R. Mizuta, and S. Kusunoki, 2009: Future change in wintertime atmospheric block-ing simulated using a 20-km-mesh atmospheric global circulation model. *Journal of Geophysi-cal Research: Atmospheres (1984–2012)*, **114 (D12)**.

39

Megann, A., and Coauthors, 2014: Go5. 0: the joint nerc–met office nemo global ocean model for use in coupled and forced applications. *Geoscientific Model Development*, **7 (3)**, 1069–1092.

Menary, M. B., D. L. R. Hodson, J. I. Robson, R. T. Sutton, R. A. Wood, and J. A. Hunt, 2015: Exploring the impact of cmip5 model biases on the simulation of north atlantic decadal variability. *Geophysical Research Letters*, n/a–n/a, doi:10.1002/2015GL064360, URL http://dx.doi.org/10.1002/2015GL064360, 2015GL064360.

Menary, M. B., W. Park, K. Lohmann, M. Vellinga, M. D. Palmer, M. Latif, and J. H. Jungclaus, 2012: A multimodel comparison of centennial Atlantic meridional overturning circulation variability. *Climate Dynamics*, **38 (11-12)**, 2377–2388, doi:{10.1007/s00382-011-1172-4}.

Nonaka, M., and S.-P. Xie, 2003: Covariations of sea surface temperature and wind over the kuroshio and its extension: Evidence for ocean-to-atmosphere feedback*. *J. Climate*, **16 (9)**, 1404–1413, doi:doi:10.1175/1520-0442(2003)16\textless1404:COSSTA\textgreater2.0.CO;2, URL http://dx.doi.org/10.1175/1520-0442(2003)16"textless1404:COSS%TA"textgreater2.0.CO;2.

Polo, I., J. Robson, R. Sutton, and M. A. Balmaseda, 2014: The importance of wind and buoyancy forcing for the boundary density variations and the geostrophic component of the amoc at 26 n. *Journal of Physical Oceanography*, **44 (9)**, 2387–2408.

Roberts, C., and Coauthors, 2013: Atmosphere drives recent interannual variability of the atlantic meridional overturning circulation at 26.5 n. *Geophysical Research Letters*, **40 (19)**, 5164–5170.

Robson, J. I., 2010: Understanding the performance of a decadal prediction system. Ph.D. thesis, The University of Reading, Reading, UK.

Rodwell, M., D. Rowell, and C. Folland, 1999: Oceanic forcing of the wintertime North Atlantic Oscillation and European climate. *Nature*, **398 (6725)**, 320–323, doi:{10.1038/18648}.

Roussenov, V. M., R. G. Williams, C. W. Hughes, and R. J. Bingham, 2008: Boundary wave communication of bottom pressure and overturning changes for the North Atlantic. *Journal Of Geophysical Research-Oceans*, **113 (C8)**, doi:{10.1029/2007JC004501}.

Sarafanov, A., A. Falina, A. Sokov, and A. Demidov, 2008: Intense warming and salinification of intermediate waters of southern origin in the eastern subpolar north atlantic in the 1990s to mid-2000s. *Journal of Geophysical Research: Oceans*, **113 (C12)**, n/a–n/a, doi:10.1029/2008JC004975, URL http://dx.doi.org/10.1029/2008JC004975.

Saravanan, R., and J. C. McWilliams, 1998: Advective ocean-atmosphere interaction: An analytical stochastic model with implications for decadal variability. *Journal of Climate*, **11 (2)**, 165–188.

Scaife, A. A., and Coauthors, 2011: Improved atlantic winter blocking in a climate model. *Geophysical Research Letters*, **38 (23)**.

Schauer, U., and A. Beszczynska-Möller, 2009: Problems with estimation and interpretation of oceanic heat transport–conceptual remarks for the case of fram strait in the arctic ocean. *Ocean Science*, **5 (4)**, 487–494.

Screen, J. A., 2013: Influence of arctic sea ice on european summer precipitation. *Environmental Research Letters*, **8 (4)**, 044 015.

Sévellec, F., and A. V. Fedorov, 2013: The leading, interdecadal eigenmode of the atlantic meridional overturning circulation in a realistic ocean model. *Journal of Climate*, **26 (7)**, 2160–2183.

Sicre, M.-A., and Coauthors, 2008: A 4500-year reconstruction of sea surface temperature variability at decadal time-scales off North Iceland. *Quaternary Science Reviews*, **27 (21-22)**, 2041–2047, doi:{10.1016/j.quascirev.2008.08.009}.

Smith, D. M., R. Eade, N. J. Dunstone, D. Fereday, J. M. Murphy, H. Pohlmann, and A. A. Scaife, 2010: Skilful multi-year predictions of atlantic hurricane frequency. *Nature Geoscience*, **3 (12)**, 846–849.

Spence, P., O. A. Saenko, W. Sijp, and M. England, 2011: The role of bottom pressure torques on the interior pathways of north atlantic deep water. *J. Phys. Oceanogr.*, **42 (1)**, 110–125, doi:doi:10.1175/2011JPO4584.1, URL http://dx.doi.org/10.1175/2011JPO4584.1.

Sutton, R., and D. Hodson, 2005: Atlantic Ocean forcing of North American and European summer climate. *Science*, **309 (5731)**, 115–118, doi:{10.1126/science.1109496}.

Timmermann, A., M. Latif, R. Voss, and A. Grotzner, 1998: Northern Hemispheric interdecadal variability: A coupled air-sea mode. *Journal Of Climate*, **11 (8)**, 1906–1931, doi:{10.1175/1520-0442-11.8.1906}.

Tréguier, A.-M., S. Theetten, E. P. Chassignet, T. Penduff, R. Smith, L. Talley, J. Beismann, and C. Böning, 2005: The north atlantic subpolar gyre in four high-resolution models. *Journal of Physical Oceanography*, **35 (5)**, 757–774.

Treguier, A. M., and Coauthors, 2014: Meridional transport of salt in the global ocean from an eddy-resolving model. *Ocean Science*, **10 (2)**, 243–255, doi:10.5194/os-10-243-2014, URL http://www.ocean-sci.net/10/243/2014/.

Tulloch, R., and J. Marshall, 2012: Exploring mechanisms of variability and predictability of atlantic meridional overturning circulation in two coupled climate models. *Journal of Climate*, **25 (12)**, 4067–4080.

Vellinga, M., and P. Wu, 2004: Low-latitude freshwater influence on centennial variability of the Atlantic thermohaline circulation. *Journal Of Climate*, **17 (23)**, 4498–4511.

Visbeck, M., H. Cullen, G. Krahmann, and N. Naik, 1998: An ocean model's response to North Atlantic Oscillation-like wind forcing. *Geophysical Research Letters*, **25 (24)**, 4521–4524, doi: {10.1029/1998GL900162}.

Volkov, D. L., T. Lee, and L.-L. Fu, 2008: Eddy-induced meridional heat transport in the ocean. *Geophysical Research Letters*, **35 (20)**, n/a–n/a, doi:10.1029/2008GL035490, URL http://dx. doi.org/10.1029/2008GL035490.

Walters, D., and Coauthors, 2011: The Met Office Unified Model global atmosphere 3.0/3.1 and JULES global land 3.0/3.1 configurations. *Geoscientific Model Development Discussions*, **4 (2)**, 1213–1271.

Wang, C., L. Zhang, S.-K. Lee, L. Wu, and C. R. Mechoso, 2014: A global perspective on cmip5 climate model biases. *Nature Climate Change*, **4 (3)**, 201–205, doi:10.1038/nclimate2118, URL http://dx.doi.org/10.1038/nclimate2118.

Watanabe, M., M. Kimoto, T. Nitta, and M. Kachi, 1999: A comparison of decadal climate oscillations in the north Atlantic detected in observations and a coupled GCM. *Journal Of Climate*, **12 (9)**, 2920–2940, doi:{10.1175/1520-0442(1999)012\textless2920:ACODCO\textgreater2. 0.CO;2}.

Wilks, D., 1997: Resampling hypothesis tests for autocorrelated fields. *Journal Of Climate*, **10 (1)**, 65–82.

Wohlleben, T., and A. Weaver, 1995: Interdecadal Climate Variability In The Subpolar North-Atlantic. *Climate Dynamics*, **11 (8)**, 459–467, doi:{10.1007/s003820050088}.

Yeager, S., 2015: Topographic coupling of the atlantic overturning and gyre circulations. *J. Phys. Oceanogr.*, doi:doi:10.1175/JPO-D-14-0100.1, URL http://dx.doi.org/10.1175/JPO-D-14-0100.1.

Yeager, S., and G. Danabasoglu, 2012: Sensitivity of atlantic meridional overturning circulation variability to parameterized nordic sea overflows in ccsm4. *Journal of Climate*, **25 (6)**, 2077–2103.

Zhang, R., 2010: Latitudinal dependence of Atlantic meridional overturning circulation (AMOC) variations. *Geophysical Research Letters*, **37**, doi:{10.1029/2010GL044474}.

Zhang, R., and T. L. Delworth, 2006: Impact of Atlantic multidecadal oscillations on India/Sahel rainfall and Atlantic hurricanes. *Geophysical Research Letters*, **33 (17)**, doi:{10.1029/2006GL026267}.

Zhang, R., and G. K. Vallis, 2007: The role of bottom vortex stretching on the path of the north Atlantic western boundary current and on the northern recirculation gyre. *Journal Of Physical Oceanography*, **37 (8)**, 2053–2080, doi:{10.1175/JPO3102.1}.

45

	NAC	Irminger Current
East advection	-1660	493
West advection	1753	-392
North advection	33	0
South advection	-83.1	-23.7
Net vertical advection	7.5	-63.9
Net convergence	51.4	15.2
Surface	-49.8	-16.9
A: Sum of advection and surface (net sum)	1.6	-1.7
B: Ocean heat content change (net actual)	0.1	0.1
Correlation A:B (Monthly, Annual, Decadal)	0.96, 0.93, 0.98	0.96, 0.94, 0.95

984   TABLE 1. Time mean simulated heat fluxes into the North Atlantic Current (NAC) and Irminger Current

985   regions (TW, referenced to 0°C).

	Monthly	Annual	Decadal
NAC $v_0 T'$	0.00 (0.01)	-0.16 (-1.1)	-0.23 (-1.6)
NAC $v' T_0$	0.29 (0.82)	0.36 (2.4)	0.42 (2.9)
Irminger Current $v_0 T'$	0.83 (0.83)	0.34 (0.66)	0.29 (0.53)
Irminger Current $v' T_0$	0.19 (0.10)	-0.10 (-0.18)	-0.14 (-0.24)

TABLE 2. Correlations (regression slopes in brackets) between net ocean heat transport (vT) and advective heat flux components in the North Atlantic Current (NAC) and Irminger Current at various timescales (TW). The 95% significance levels, assuming a two-tailed t-test and accounting for some missing data, are 0.03, 0.12, and 0.37 for monthly, annual, and decadal data respectively.

	Monthly	Annual	Decadal
NAC v_0T'	139	43	31
NAC $v'T_0$	149	44	33
NAC $v'T'$	58	16	11
Irminger Current v_0T'	13.1	4.0	3.2
Irminger Current $v'T_0$	6.7	3.6	2.7
Irminger Current $v'T'$	4.0	1.1	1.0

990 TABLE 3. Standard deviations of advective heat flux components in the North Atlantic Current (NAC) and
991 Irminger Current at various timescales (TW).

Mean state	Density change for one s.d. change in T	Density change for one s.d. change in S
EN4 + HG3 bias	0.027	0.014
EN4 + IPSL bias	0.010	0.014
EN4 (original)	0.023	0.014

TABLE 4. Characteristic magnitudes of density changes (kg/m^3) in different simulated/estimated temperature or salinity (T/S) regimes. Mean states are volume averaged temperature and salinity (in the models defined as the observed mean plus a model bias, *e.g.* EN4 + HG3 bias) in the Irminger Current (43–45°W, 58–60°N, top 500m). The density changes are calculated by estimating the decadal standard deviation (s.d.) in temperature or salinity (by band-pass filtering the data to allow only periods in the range 10–30 years) and recalculating the densities with these T/S perturbations added. As there is limited raw data from EN4 to reliably estimate decadal variability in the Irminger Current, and to simplify the experimental design and interpretation, we use HG3 estimates of the decadal variability in temperature and salinity in all cases.

LIST OF FIGURES

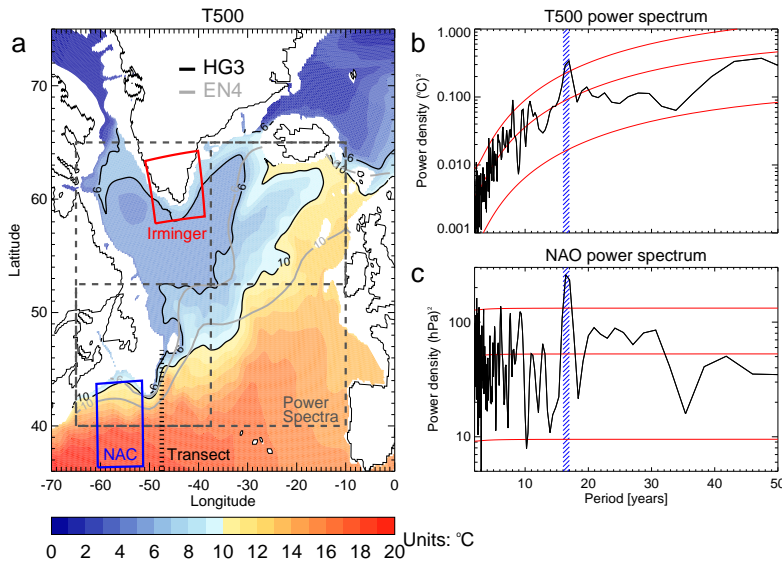|	Study	Period (years)	Mechanism
1	Delworth '93	50	Ocean
2	Timmermann '98	35	Coupled
3	Grotzner '98	17	Coupled
4	Visbeck '98	12-16	Ocean*
5	Watanabe '99	~10	Ocean*
6	Dong '01	-	-
7	Eden '01	12-18	Coupled
8	Holland '01	20	Ocean
9	Eden '03	16	Ocean*
10	Dai '05	24	Ocean
11	Dong '05	25	Ocean
12	Álvarez-Garcia '08	24	Ocean*
13	Danabasoglu '08	21	-
14	Frankcombe '10	20-30	Ocean
15	Born '12	15-20	Ocean
16	Sevellec '13	24	Ocean
17	Escudier '13	20	Ocean
18	Kwon '14	20 "regime 1"	Ocean*

FIG. 1. A summary of some of the literature on simulated decadal variability in the North Atlantic subpolar gyre (NA SPG), with a particular emphasis on studies which found self-sustaining cyclical behaviour. Key regions of the NA SPG are marked. The figure legend (right) denotes the studies which we have attempted to synthesise and an associated numerical identifier. Where these studies report a significant peak in the power spectrum on decadal timescales this is noted as well as whether the mechanism is primarily ocean-only or inherently coupled. Studies where the atmosphere is postulated to amplify — but not transmute — the signal are marked with an asterisk. For each study the feedback or process which is reported as crucial in setting the timescale is marked on the map using a simple numbering system. These comprise: 1) Feedbacks relating to the deep water pathways and their interaction with the northward flowing western boundary current, 2) Rossby wave (or sometimes 'geostrophic self advection') transit times across the NA SPG, 3) the mean advection timescale for anomalies to propagate into the NA SPG from the tropics, or for small anomalies to integrate up over time. Lastly, using the same numerical key, the studies are split into which of temperature or salinity is reported to control decadal timescale density changes in the Labrador Sea. In all case, studies in brackets appear in more than one category. This represents a drastic simplification of each of these studies and the reader is referred to the original works for further details. In particular, the reported feedback/process that sets the overall timescale to some degree also reflects the precise focus of the particular study.
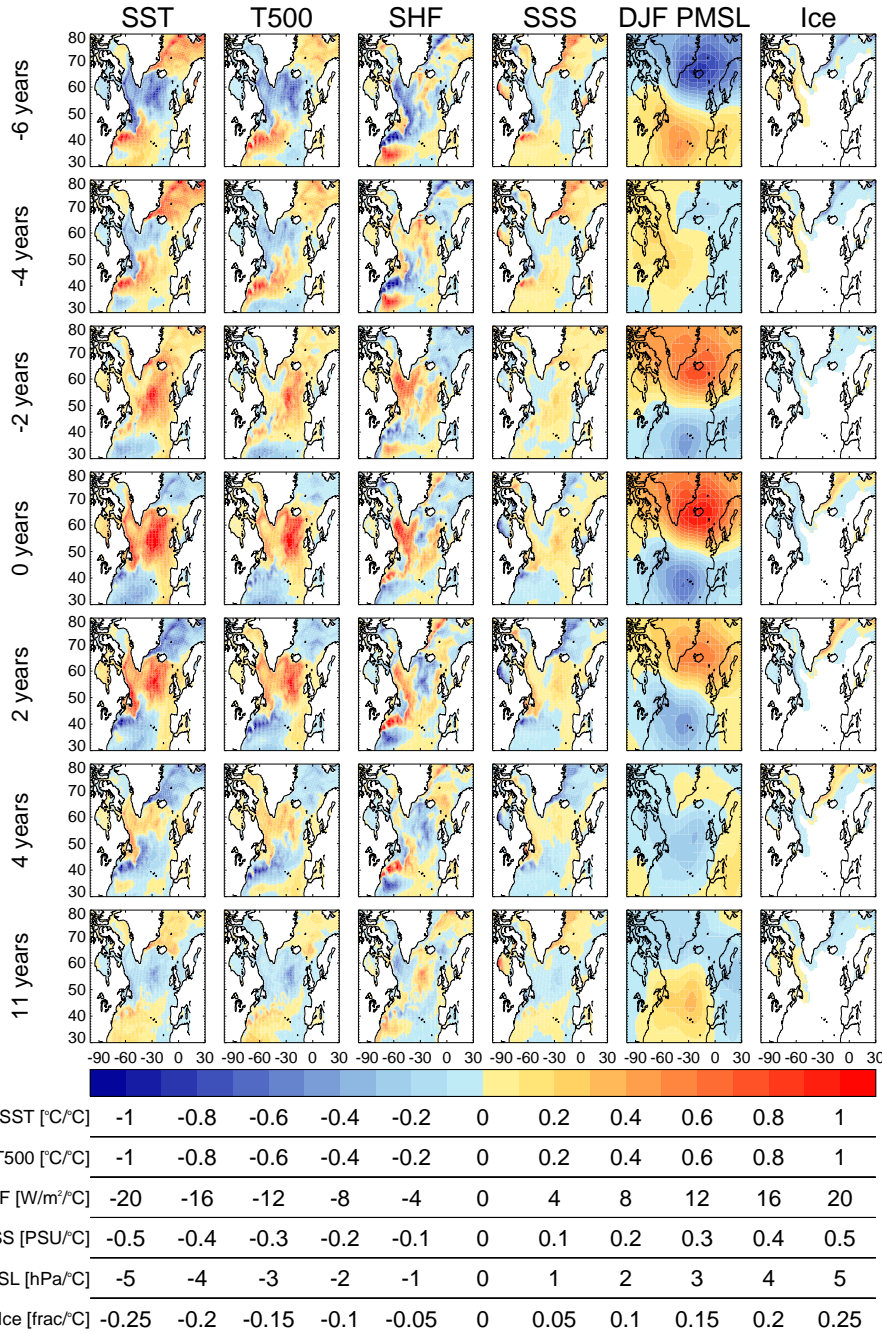
53

FIG. 2. Top 500m depth averaged temperature (T500, a) salinity (S500, b), and density (ρ500, c) biases in HG3 (computed from full time series) compared to EN4. Grey shading is used for regions shallower than 500m. d) Standard deviation in March mixed layer depths (Kara et al. 2000), to highlight where deep convection occurs
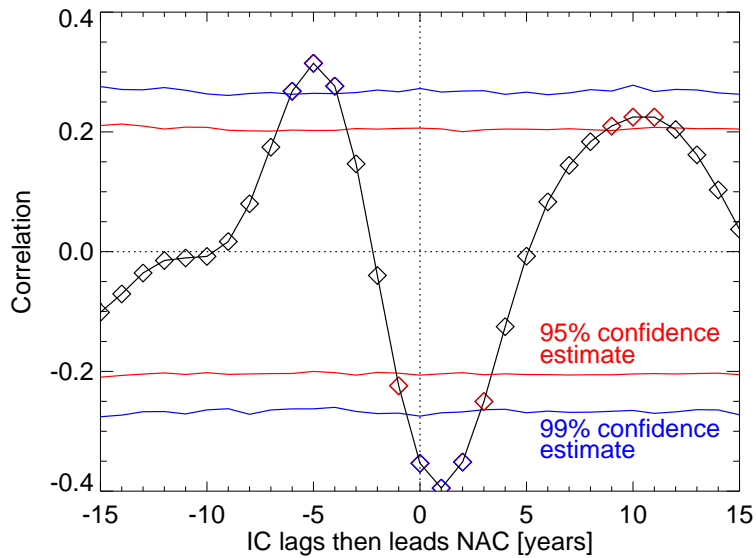
FIG. 3. a) Time mean Atlantic overturning streamfunction in HG3. The contour interval is 2Sv and the zero-line is marked with a grey contour. At 26.5°N the profile from the RAPID array is overlaid on the same colour/contour scale. The depth of the maximum in the RAPID profile is marked with a cross. Note that the latitudes north of 45°N are approximate (within 1°) due to the increasingly curved nature of the model grid towards the two northern poles. b) Time mean NA SPG barotropic streamfunction in HG3. Contour interval is 10Sv. c) Time series of the overturning streamfunction at 26.5°N and 1000m in HG3 (red). Also shown are the time mean and annual mean standard deviation from the 10 years of RAPID data (black). d) Time series of the minimum (multiplied by -1) of the barotropic streamfunction in the NA SPG in HG3.

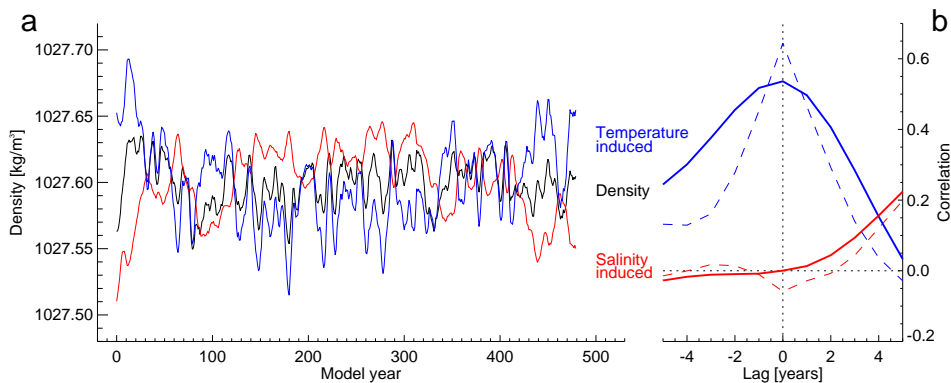FIG. 4. a) Time mean top 500m depth averaged temperature (T500) in HG3. Contours at 6°C and 10°C are also marked (black) to show the shape of the gyre and for comparison with equivalent contours from EN4 (grey). Areas in white are shallower than 500m. The dashed grey box denotes the four quadrants and fifth overall region for which power spectra of T500 were produced. The Irminger Current region (red box) and Gulf Stream/North Atlantic Current region (blue box) analysed in the text are also marked. The dashed black line stretching south from the Grand Banks denotes the transect location for dynamic height analysis. b) The T500 power spectrum for the whole subpolar gyre region (combination of all four quadrants). An estimate of significance is given by the 5–95% confidence intervals for a red noise process with the same mean and standard deviation. Periods of 16–17 years are highlighted with the blue shading. c) As (b) but for the NAO index, defined as the difference between simulated sea level pressures over the Azores and Iceland.
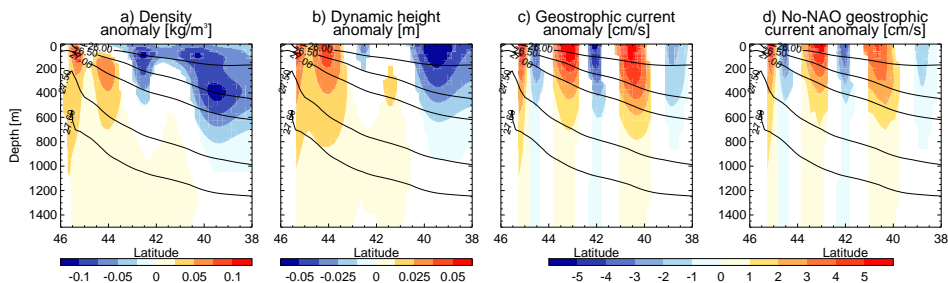
FIG. 5. Regressions between basin-wide North Atlantic (45–65°N) sea surface temperatures (SSTs) and, from left to right: SST, top 500m depth averaged temperature (T500), net surface heat flux into ocean (SHF), sea surface salinity (SSS), wintertime mean sea level pressure (DJF MSLP), and ice fraction. From top to bottom, the SST index lags then leads the fields from -6 to +4 and then +11 years. The same colour palette is used for each regression map with the units and scale for each regression slope shown below.
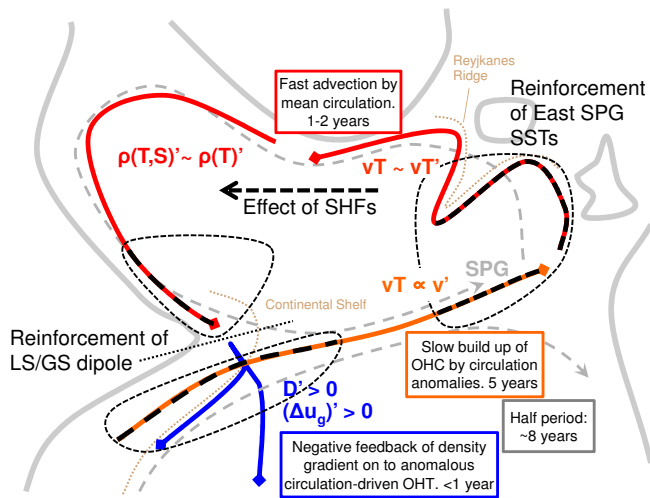
FIG. 6. The lagged correlation between the Irminger Current and North Atlantic Current top 500m depth averaged temperatures (T500). Regions are as marked in Figure 4a. Time series have been filtered with a band-pass filter of 5–150 years to highlight the decadal correlations by removing annual variability and the long term drift. An estimate of the significance is provided by the 95% (red) and 99% (blue) confidence intervals estimated by creating 40,000 random time series with the same mean, standard deviation, and applied filtering.
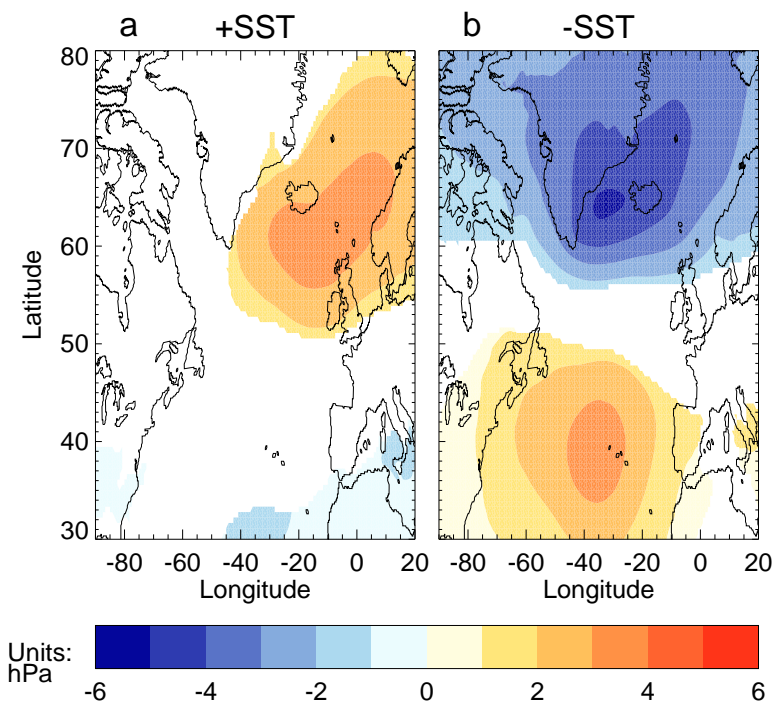
FIG. 7. a) 5-year smoothed Labrador Sea (50–60°W, 55–62°N) top 500m mean density (black) and contributions from temperature (by keeping salinity at the time mean in the density equation of state, blue) and from salinity (by keeping temperature at the time mean in the density equation of state, red). Temperature and salinity both linearly detrended prior to computing density. b) Lagged correlation of temperature-induced (blue) and salinity-induced (red) density against actual density for detrended data, either unsmoothed (dashed) or pre-smoothed with a 5-year running mean (solid, as in (a)). Temperature/salinity-induced density leads actual density at negative lags.
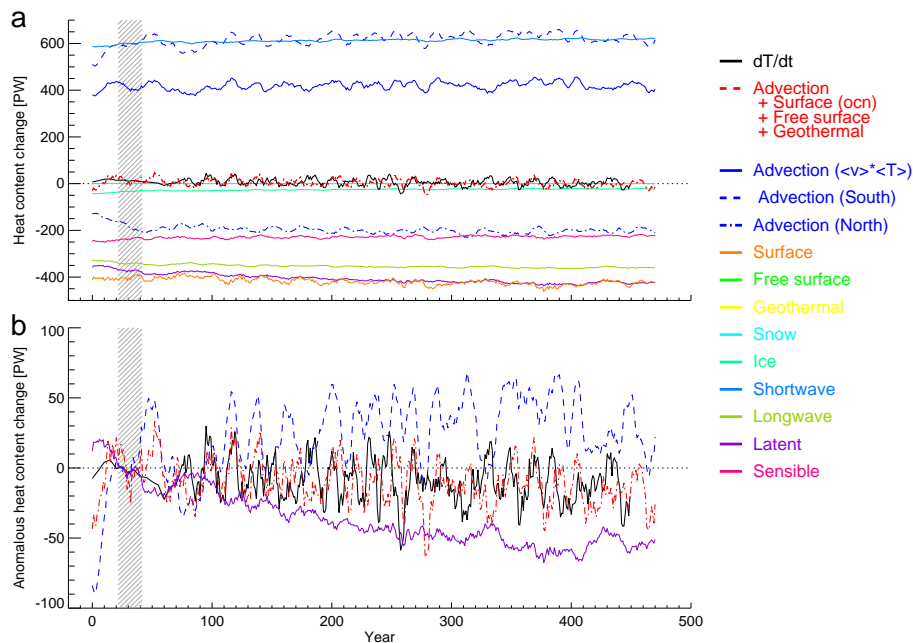
59

FIG. 8. Transect south from the Grand Banks through the North Atlantic Current at 47.5°W, as shown in Figure 4a. Density (referenced to 0m) composite of high minus low densities in the Labrador Sea, computed by averaging all cases where Labrador Sea volume mean density (computed over the region 47–55°*W*, 56–61°, 0–1000m) was at least one standard deviation larger than the time mean, and subtracting the average of all cases where density was at least one standard deviation less than the time mean. Cross sections lag by 1 year the Labrador Sea index. b) As (a) but for dynamic height composites (relative to 1500m). c) As (a) but for the geostrophic circulation (relative to 1500m). d) As (c) but first removing the NAO signal from the density field after Polo et al. (2014), see text. Cross-sectional time mean density is indicated by the black contours. All data has been detrended and 5-year smoothed. Only data significant at the 99% level is shown. Significance is estimated using a moving blocks bootstrap approach (Wilks 1997) reconstructing the composites 10000 times by resampling the data with a block length estimated from the autocorrelation in each original composite.

FIG. 9. A schematic of the proposed mechanism. The various processes in different regions, the timescales, and the postulated role of the atmosphere are as described in the text. Dashed grey lines denote the approximate location of NA SPG and subtropical gyres with bathymetry of particular interest marked brown. Also marked are regions where ocean heat transport correlates with circulation anomalies (orange) or is dominated by temperature anomalies (red) and where the negative feedback is suggested to occur (blue). Additionally, black dashed lines denote regions where the atmosphere is postulated to play a role in forcing or feeding back on ocean anomalies.

FIG. 10. Mean sea level pressure (MSLP) composites created using area-averaged eastern NA SPG SSTs (10–30°W, 50–65°) to highlight the asymmetry between positive and negative phases of the proposed mechanism. a) Composite created using the highest 10% of SST anomalies. b) As (a) but for the lowest 10% of SST anomalies. Only data significant at the 99% level is shown. Significance is estimated using a moving blocks bootstrap approach (Wilks 1997) reconstructing the composites 10000 times by resampling the data with a block length estimated from the autocorrelation in each original composite.

FIG. 11. The full depth heat budget of the NA SPG (53–73°N) volume plotted using 9 year running means for clarity and to highlight decadal variability. Positive is into the specified region. a) Individual components of the heat budget as denoted in the legend. b) The anomalous heat budget (referenced against years 22–42) to highlight the trends in latent heat fluxes and advective heat fluxes through the southern boundary. Note that the heat content change ($\frac{dT}{dt}$, black) and sum of heat fluxes (red) do not match prior to the year 100 as instantaneous ocean temperatures (used to calculate $\frac{dT}{dt}$) were stored with intermittent frequency during this period.